Article

Not peer-reviewed version

The Role of C2 Domains in Two Different Phosphatases: PTEN and SHIP2

Laura John , Fiona Naughton , Mark Sansom , Andreas Haahr Larsen *

Posted Date: 16 February 2023

doi: 10.20944/preprints202302.0282.v1

Keywords: PTEN; SHIP2; C2 domain; Ptase domain; MD

Article

The Role of C2 Domains in Two Different Phosphatases: PTEN and SHIP2

Laura John [1], Fiona Naughton [1,2], Mark S. P. Sansom [1] and Andreas Haahr Larsen [1,3,*]

[1] Department of Biochemistry, University of Oxford, OX1 3QU Oxford, UK
[2] Current address: Cardiovascular Research Institute, University of California San Francisco, San Francisco, California 94143, USA
[3] Department of Neuroscience, University of Copenhagen, 2200 Copenhagen, Denmark
* Correspondence: andreas.larsen@sund.ku.dk

Abstract: Phosphatase and tensin homologue (PTEN) and SH2-containing-inositol-5'-phosphatase 2 (SHIP2) are structurally and functionally similar. They both consist of a Phosphastase (Ptase) domain and an adjacent C2 domain, and both proteins dephosphorylate phosphoinositol-tri(3,4,5)phosphate, PI(3,4,5)P_3; PTEN at the 3-phophate and SHIP2 at the 5-phosphate. Therefore, they play pivotal roles in the PI3K/Akt pathway. Here, we investigate the role of the C2 domain in membrane interactions of PTEN and SHIP2, using molecular dynamics simulations and free energy calculations. It is generally accepted that for PTEN the C2 domain interacts strongly with anionic lipids and therefore significantly contributes to membrane recruitment. In contrast, for the C2 domain in SHIP2 we previously found much weaker binding affinity for anionic membranes. Our simulations confirm the membrane anchor role of the C2 domain in PTEN, as well as its necessity for the Ptase domain in gaining its productive membrane binding conformation. In contrast, we identified that the C2 domain in SHIP2 undertakes neither of these roles, which are generally proposed for C2 domains. Our data support a model in which the main role of the C2 domain in SHIP2 is to introduce allosteric interdomain changes that enhance catalytic activity of the Ptase domain.

Keywords: PTEN; SHIP2; C2 domain; Ptase domain; MD

1. Introduction

C2 domains are structurally conserved modules of about 130 residues, which folds as a beta-sheet sandwiches [1]. C2 domains are often considered as membrane anchors, but may play alternative or additional roles in membrane-located signalling proteins. The phosphatase and tensin homologue (PTEN) and SH-containing-inostitol-5-phospatase 2 (SHIP2) are both phosphatases. They function by dephosphorylating phosphoinositol-tri(3,4,5)phosphate, PI(3,4,5)P_3 to form PIP_2 [2] (Figure 1). The product of PTEN dephosphorylation is phosphoinositol-di(4,5)phospate (PI(4,5)P_2), whereas SHIP2 forms PI(3,4)P_2. This process is part of several signalling cascades [3]. The presence of PIP_3 promotes proliferation of the cell, so by removing PIP_3 from the membrane, PTEN acts as a tumour suppressor, and mutations of the PTEN gene are associated with cancer [4].

Both PTEN and SHIP2 consist of an N-terminal phosphatase (Ptase) domain, followed by a C2 domain. The Ptase domain contains the active sites, whereas the C2 is an auxiliary domain, and is widely believed to facilitate membrane binding, in SHIP2 and PTEN as well as in several other protein classes [5]. Therefore, we were surprised by our previous coarse-grained molecular dynamics (MD) simulations, which showed that the C2 domain of SHIP2 ($C2_{SHIP2}$) bound only weakly to a lipid bilayer mimicking mammalian inner membranes [6]. In all-atom MD, $C2_{SHIP2}$ even dissociated from the membrane, verifying the weak lipid binding. Those preliminary results challenge the conception of C2 as a membrane anchor, at least in the case of SHIP2. In this study, we therefore investigated the role of $C2_{SHIP2}$ and compared it with the corresponding domain of the related protein PTEN. We used

 doi:10.20944/preprints202302.0282.v1

MD simulations to study the protein complexes containing both Ptase and C2 domains (here denoted full-length PTEN or SHIP2), as well as the isolated Ptase domains. The results can be directly compared with the previous simulations of isolated C2 domains of the two proteins [6], as we used the same simulation setup, i.e., lipid composition, simulation duration, and number of repeats, etc (see Methods).

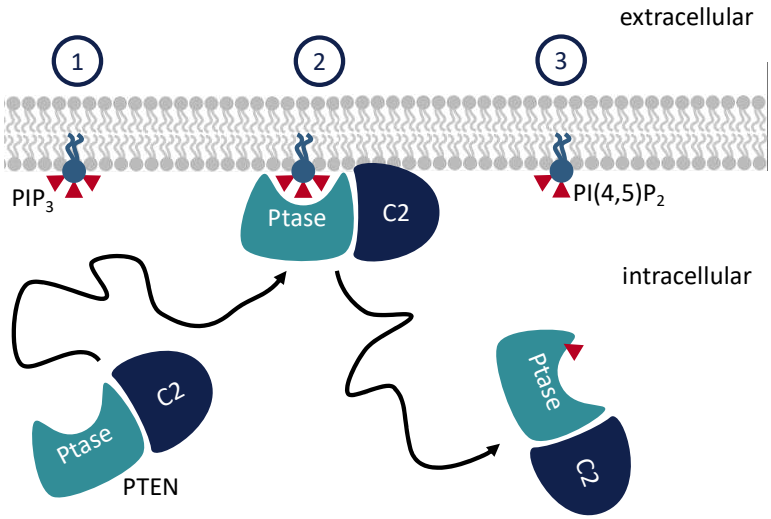

Figure 1. The function of PTEN. PTEN binds the inner leaflet of plasma membrane and dephosphorylates PI(3,4,5)P_3 to form PI(4,5)P_2. SHIP2 works similarly, but the product is instead PI(3,4)P_2. Adapted from Ref [7].

2. Methods

2.1. Preparing initial structures: addition of missing residues

Full-length PTEN consisted of residues 1-403, whereof the structure of residues 14-281 and residues 312-351 was taken from the X-ray crystal structure (PDB 1D5R) [8]. The missing N-terminal residues 1-13 were modelled as a helix, using Modeller [9]. Missing residues 282-311 and C-terminal residues 352-403 were modelled as loops, also using Modeller [9].

We previously simulated lipid binding of a Ptase-C2 core of PTEN [6], but that was without the N-terminal helix. $Ptase^{PTEN}$ consisted of residues 1-186 and $C2^{PTEN}$ of residues 191-352 of the full-length construct.

Full-length SHIP2 was simulated previously [6], and consisted of residues 418-878. The structure of residues 420-731 and residues 745-874 was taken from chain B of the X-ray crystal structure (PDB 5OKM) [10]. The missing residues 418-419, 732-744, and 875-878 were modelled as loops, using Modeller [9]. $Ptase^{SHIP2}$ consisted of residues 418-729 and $C2^{SHIP2}$ of residues 747-862 of the full-length construct.

2.2. Coarse-grained MD simulations

The initial structures were rotated through a random angle, then centred before they were transformed into a coarse-grained model following the Martini 2.2 coarse graining scheme [11], using the *martinize* script [12]. An elastic network was applied to the protein, with default settings and secondary structure was given as input using the DSSP algorithm [13]. The protein was inserted 4.4 nm above a lipid bilayer using the *insane* script [14]. The membrane consisted of 80% POPC, 15% POPS and 5% $POPIP_2$ (Martini lipid POP2 [15]) (see lipid topologies at www.cgmartini.nl). The lipid headgroup is based on PIP(3,4)P_2 [15]. The insane script also solvated the protein and membrane in 90% Martini water, with 10% antifreeze particles [11] and neutralized the system with Na^+ or Cl^- ions. For $Ptase^{SHIP2}$ simulations, the box was 10x10x20 nm^3, for $Ptase^{PTEN}$ simulations, the box was 7x7x18 nm^3 and for full-length simulations, the box was 12x12x24 nm^3. The simulations were performed

 doi:10.20944/preprints202302.0282.v1

using the Martini 2.2 force field [12]. The use of Martini 2.2 made it possible to compare the results directly with previous simulations [6]. The configuration was minimized with a steepest descend algorithm. Van der Waals and Coulomb cut-offs were both 1.1 nm, so four times less than the initial distance between protein and membrane. The system was equilibrated for 10 ns with a 20 fs timestep in the NPT ensemble, with a semi-isotropic Berendsen barostat [16] set at 1 bar with a time constant of 1 ps and compressibility of 0.3 $kbar^{-1}$, and v-scale thermostat [17] set at 323 K with a time constant of 1 ps. The simulations were constrained using the LINCS algorithm [18]. After equilibration, simulations were run for 2 μs with a 35-fs time step and the same settings as the equilibration. All coarse-grained simulations were repeated 25 times.

2.3. All-atom MD simulations

The coarse-grained binding poses were converted to all-atom models using CG2AT [19] (version 0.2). The all-atom simulations were run with the CHARMM36m force field [20] with TIP3P water. Cut-off distances for van der Waals and Coulomb forces were 1.2 nm. Long-range electrostatics were handled by the Particle Mesh Ewald algorithm [21]. The system was first minimized, then equilibrated in the NVT ensemble for 100 ps and with a 2-fs time step. A v-rescale thermostat [17] was applied to keep the temperature at 300 K, with a time step of 0.1 ps. The system was subsequently equilibrated for 100 ps with a 2-fs time step in the NPT ensemble, using a Parinello-Rahman semi-isotropic barostat [22] to keep pressure at 1 bar, with time constant of 5 ps and compressibility of 0.045 $kbar^{-1}$. In both equilibration simulations, the protein atoms were position restrained by a force constant of 1000 kJ/mol in all directions. Finally, a 600 ns production run was generated with a 2-fs time step and without position restraint on the protein.

2.4. Analysis of coarse-grained simulations

The distance between the protein center of mass and the membrane center of mass (after centring of the protein in the box) was calculated with the GROMACS algorithm *gmx distance*. The *zz* component of the rotational matrix (R_{zz}) was calculated with *gmx rotmat*. Binding poses were selected from the frequency densities in the R_{zz} vs distance 2D landscapes.

2.5. Analysis of all-atom MD simulations

The center-of-mass distance was calculated with the *gmx distance* tool and minimum distances by *gmx mindist*. Root mean square deviations (RMSD) were used to monitor the difference between the binding pose of isolated Ptase and Ptase in the full-length Ptase-C2 complex bound to the same lipid membrane. The RMSD were calculated after alignment in the *xy*-plane (i.e. the approximate bilayer plane) and around the *z*-axis using an in-house script. RMSD was also used to monitor the structural change after converting the coarse-grained binding pose to all-atom structure and simulating it in the CHARMM-36m all-atom force field [20] with TIP3P water. In that case, the frames were compared to the initial frame in the atomistic simulation and RMSDs were calculated with GROMACS, using *gmx rms*. Finally, RMSD was used to compare the SHIP2 full-length and the $Ptase_{SHIP2}$ simulation with a previously reported crystal structure, respectively [10]. For this, the RMSDs were calculated per residue as time averages over the 600 ns simulations, with the initial frame as reference structure, using *gmx rmsf*. For the same simulations, root mean square fluctuations (RMSFs) were used to monitor fluctuations of regions in the Ptase domain of SHIP2 during the 600-ns simulations. These were likewise calculated with *gmx rmsf*.

2.6. Free energy calculations

Binding poses from the coarse-grained simulations were taken as initial structures. These were then pulled away from the membrane, along the *z*-coordinate using the GROMACS pull code. A pull rate of 0.2 nm/ns with a harmonic (umbrella-type) constraint with a force constant of 1000 kJ/mol/nm^2. The binding pose was likewise pushed 0.24 nm closer to the membrane center, with the same settings, except that the rate was inverted to be -0.2 nm/ns. Frames with distance of 0.05 nm were taken from

 doi:10.20944/preprints202302.0282.v1

the push and pull trajectories, ranging from the frame where the protein was pushed 0.24 nm closer to the membrane center of mass than the binding pose, to a frame where the protein was pulled to a distance of 7 nm (for Ptase simulations) or 8.5 nm (for full-length simulations) from the membrane center of mass. Position restraints were applied on all lipids in the pull simulations (not in the push simulations or umbrella simulations) to prevent lipids being pulled out of the membrane together with the protein. Each frame (window) was sampled for 1 μs with a timestep of 35 fs, without position restraint on the lipids. Potential of mean force (PMF) was calculated from the forces using the WHAM algorithm [23], as implemented in GROMACS by the command *gmx wham* [24], omitting the first 100 ps from the analysis. Bootstrapping using 200 repeats was used to estimate the standard deviation [24].

We wished to obtain the free energy contributions for C2 and Ptase in the full-length binding mode, respectively. To this mean, Ptase and C2 from full-length PTEN were extracted, each domain was then placed back by the membrane and resolvated. The same was done for Ptase and C2 from SHIP2. The GROMACS function *gmx trjconv* was used for extraction. Resolvation was done with insane using the same box size as the box from which the protein was extracted. Topology files were changed manually to accommodate the changes. The system was minimized and equilibrated in the NPT ensemble for 10 ns, with a time step of 30 fs and with the protein restrained by a 1000 kJ/mol/nm^2 force constant. Umbrella sampling was then performed as described above.

2.7. Visualization and plotting

Structures were visualized using PyMOL (The PyMOL Molecular Graphics System, Version 1.2r3pre, Schrödinger, LLC), plots were generated in Python3, using Numpy [25] and Matplotlib [26].

2.8. Reproducibility and data availability

Scripts for running the simulations are available at GitHub, https://github.com/andreashlarsen/Larsen2023-Ptase.

3. Results

3.1. N-terminal helix in PTEN participates in lipid-binding

Initially, we focussed on full-length PTEN and SHIP2. We had simulated these constructs previously [6], but we made new simulations for full-length PTEN to include an N-terminal helix in Ptase$_{\text{PTEN}}$, which was not modelled in the PTEN structure in Ref [6]. 25 coarse-grained simulations were performed on full-length PTEN with the N-terminal helix. To map out the "binding-landscape", we plotted the center of mass-distance from membrane to C2 domain against R_{zz}. R_{zz} is the zz-component of the rotation matrix with respect to a reference structure, in this case, the last frame of the first repeat. Thus, R_{zz} represents a difference in binding orientation. Two binding modes were observed (Figure 2A), but only one was productive, i.e., with the catalytic active site of the Ptase domain in contact with the membrane [6]. The N-terminal helix contributed to the lipid binding in the productive binding mode, by insertion into the lipid bilayer (Figure 2B). The productive binding mode was, however, very similar to the productive mode for simulations of PTEN without the N-terminal helix (Figure 2B) (from Ref [6]), except for a tilt that allowed deeper helix insertion.

Preprints.org (www.preprints.org) | NOT PEER-REVIEWED | Posted: 16 February 2023 doi:10.20944/preprints202302.0282.v1

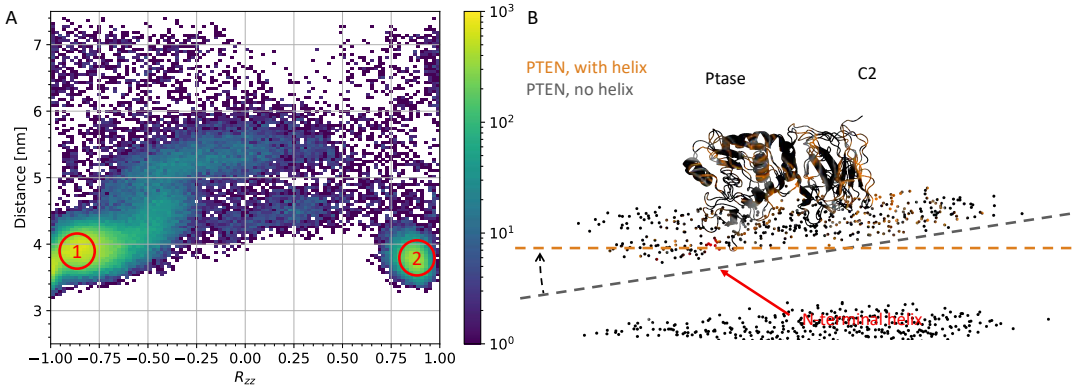

Figure 2. The role of the N-terminal helix of PTEN. (A) R_{zz} vs protein-membrane center-of-mass distances for 25 repeats of coarse-grained simulations of full-length PTEN with N-terminal helix. Two binding modes were observed (red circles), with mode 1 being the productive mode, as shown in panel B, and mode 2 being unproductive, i.e., the active site of the Ptase domain was pointing away from the membrane (not shown). (B) Alignment of PTEN productive binding mode (orange, helix in red), with the productive mode of PTEN without the N-terminal helix (grey). Alignment was done after conversion from coarse-grained to all-atom resolution. Bilayer planes are shown (dashed lines) together with phosphates from the lipid headgroups (spheres).

3.2. Membrane binding of isolated Ptase from PTEN and SHIP2

We did 25 repeats of 2-μs coarse-grained simulations of $\text{Ptase}_{\text{PTEN}}$ to investigate the different lipid binding modes of Ptase in the absence of C2. Using these simulations, the binding landscape could be mapped out, as done for full-length PTEN (Figure 2A). However, this time the Ptase conformation from the productive binding mode of the full-length PTEN was used as reference structure. Therefore, $R_{zz} = 1$ means that the simulated Ptase domain has the same orientation as the Ptase domain from the full-length binding mode, whereas $R_{zz} = -1$ corresponds to a 180° rotation. Three binding modes were observed (Figure 3A and 3C). None of the observed modes were identical to Ptase of the full-length PTEN simulation (Figure 3D), with a minimum RMSD of 0.9 nm for mode 3.

We also did 25 repeats of 2-μs coarse-grained simulations of $\text{Ptase}_{\text{SHIP2}}$ and compared the binding conformations to the Ptase binding-conformation of the full-length SHIP2 simulation [6]. In this case, we only observed two binding modes (Figure 3B and 3E). Mode 2 resembled that of Ptase from full-length SHIP2 closely (Figure 3F), with an RMSD of 0.2 nm.

Preprints.org (www.preprints.org) | NOT PEER-REVIEWED | Posted: 16 February 2023 doi:10.20944/preprints202302.0282.v1

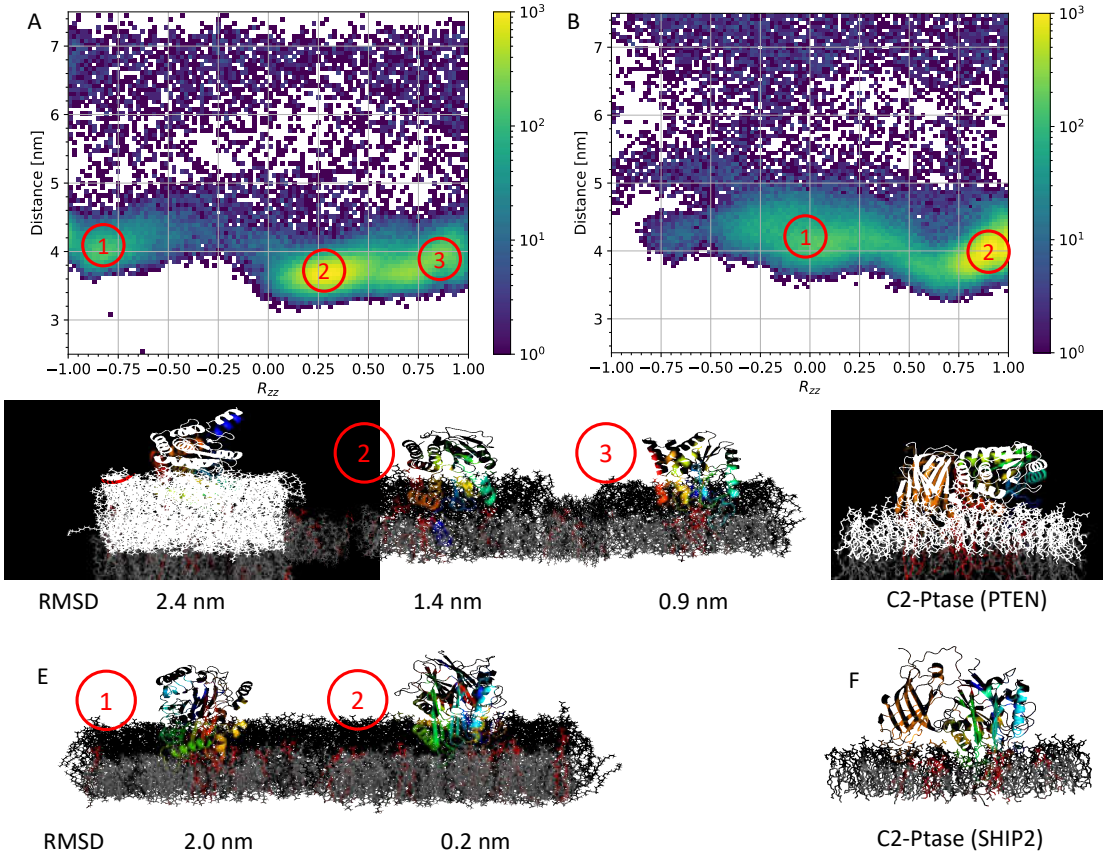

Figure 3. Simulations of isolated Ptase domains binding to lipid membrane. (A) Density map for 25 simulations of $Ptase_{PTEN}$. The center of mass-distance between $Ptase_{PTEN}$ and the lipid bilayer is plotted against the orientation with respect to Ptase of full-length PTEN. R_{zz} = 1 means the orientation is the same and R_{zz} = -1 corresponds to a 180° rotation. Dominant binding modes are numbered. (B) As panel A, but for simulations of $Ptase_{SHIP2}$. (C) Dominant binding modes for $Ptase_{PTEN}$, with corresponding RMSD values with respect to Ptase of the full-length PTEN simulation. (D) Dominant binding mode for full-length PTEN. (E) Dominant binding modes for $Ptase_{SHIP2}$. (F) Dominant binding mode for full-length SHIP2. All proteins are shown in rainbow colour scheme, from blue in the N-terminus, over green, yellow, and orange to red in the C-terminus. PC lipids are grey, PS are black, and PIP_2 are red.

3.3. Free energy calculations

The final full-length binding conformations of PTEN and SHIP2 were used for free energy calculations. First, we performed umbrella sampling and potential of mean force (PMF) calculations for unbinding of full-length PTEN and SHIP2 from the lipid membrane. The binding energy (ΔPMF) was calculated as the difference between the PMF minimum and the PMF in bulk (Figure 4). The binding energy of PTEN was estimated to be -162 ± 1 kJ/mol, and the binding energy of SHIP2 was estimated to be substantially smaller, namely -96 ± 2 kJ/mol.

We also analysed the contribution from C2 and Ptase, respectively, to the binding energy of the full-length complexes. To this mean, we first removed C2 from the full-length PTEN productive binding mode, so only Ptase was left in its binding mode. We then calculated the free energy of unbinding for the Ptase domain. The same was done for all four domains, i.e., for C2 and Ptase from PTEN and SHIP2 (Figure 4B). For PTEN, the Ptase domain and the C2 domain contributed equally to the total binding energy. For SHIP2, on the other hand, the contribution from Ptase to the total binding energy was almost 3-fold higher than the contribution from the C2 domain.

The energy contribution from $PTEN_{Ptase}$ was 103 kJ/mol and the contribution from $PTEN_{C2}$ was 109 kJ/mol (only magnitudes are given for simplicity, therefore the sign is omitted). This adds up 212

 doi:10.20944/preprints202302.0282.v1

kJ/mol, i.e., 30% more than the estimated free energy of binding of full-length PTEN, which was 163 kJ/mol. Correspondingly, for SHIP2, the sum of the free energies from the components was 105 kJ/mol, which is 9% more than the estimated free energy of binding of full-length SHIP2, which was 96 kJ/mol. The higher degree of freedom of movement for the single domains (which are not constrained by neighbouring domain) may lead to this difference, through higher entropy and more optimal alignment with the membrane.

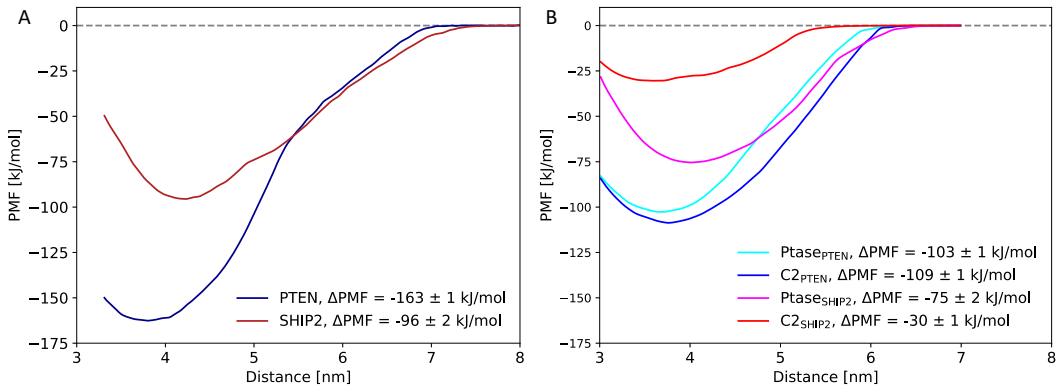

Figure 4. Binding energies as estimated by the potential of mean force. (A) Full-length PTEN (blue) and SHIP2 (red). Shaded areas show one standard deviation spread. (B) Ptase (light blue) and C2 (dark blue) from full-length PTEN. Ptase (purple) and C2 (red) from full-length SHIP2. Mean ± 1 standard error, estimated by bootstrapping [24]. Binding energy (ΔPMF) was defined as the difference between the minimum PMF value and the value in bulk.

3.4. Atomistic simulations of full-length structures

We converted the full-length binding conformations of PTEN and SHIP2 to atomistic resolution and performed a 600 ns all-atom simulation. For PTEN, we observed an RMSD from first to last frame of about 0.8 nm (Figure 5A). From visual inspection, this comes partly from loops being less compact (Figure 5D), but we also observed that the C2 and Ptase domains of PTEN shifted away from each other (Figure 5C). Moreover, the center of mass of PTEN moved away from the membrane by about 0.5 nm (Figure 5B), indicating less membrane insertion. However, the protein stayed bound throughout the simulations, and the number of contacts between both domains and PIP_2s in the membrane stayed constant (Figure 5F). A contact is here defined as a minimum distance of less than 0.6 nm [27].

For SHIP2, the RMSD between first and last frame was minor, only 0.3 nm (Figure 5A). Also, there was only a minor shift away from the membrane, between 0.1 and 0.4 nm during the simulation (Figure 5B). Also, PIP_2s stayed bound to the complex throughout the simulation, but notably, no PIP_2 was bound to the C2 domain, except in the Ptase-C2 junction (Figure 5E and F), which could explain that this domain had the smallest contribution to the binding energy (Figure 4B).

Preprints.org (www.preprints.org) | NOT PEER-REVIEWED | Posted: 16 February 2023 doi:10.20944/preprints202302.0282.v1

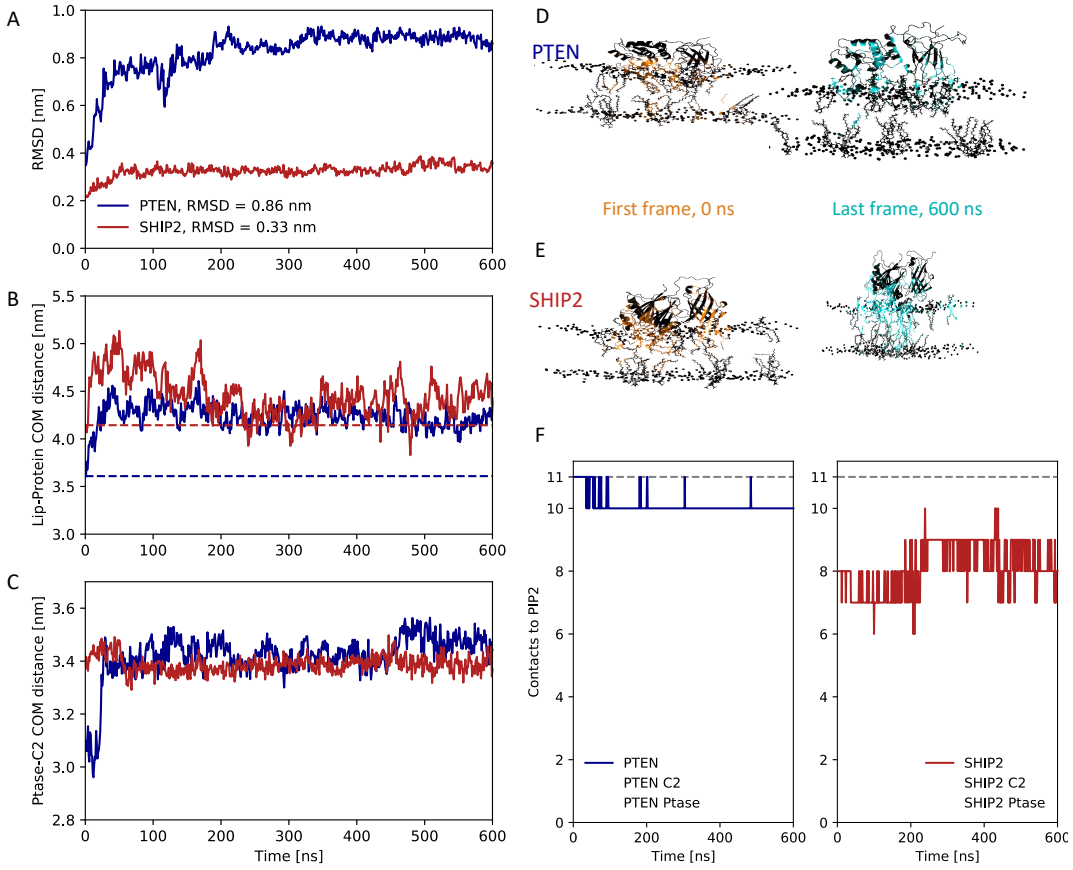

Figure 5. Atomistic simulations of full-length PTEN and SHIP2. (A) RMSD with respect to the binding poses from the coarse-grained simulations of PTEN and SHIP2. (B) Center-of-mass (COM) distance between membrane and proteins. Dashed lines show the distances for the initial coarse-grained binding poses. (C) Center-of-mass distance between C2 and Ptase domains for PTEN and SHIP2. (D) First (orange, 0 ns) and last (light blue, 600 ns) frames of the all-atom simulation of PTEN. Phosphate beads from the lipid heads are shown in grey. (E) First (orange, 0 ns) and last (light blue, 600 ns) frame from the SHIP2 all-atom simulation. (F) Number of contacts (with minimum distance less than 0.6 nm) between PIP_2 lipids and PTEN, SHIP2 or their C2 or Ptase domains. There were 11 PIP_2 lipids in the upper membrane leaflet, so this was the maximum possible number of contacts. A PIP_2 can be simultaneously in contact with C2 and Ptase if positioned at the junction.

3.5. Dynamics of full-length SHIP2 vs Ptase$_{SHIP2}$

The Ptase$_{SHIP2}$ constructive binding mode (Figure 3, mode 2) was also converted to all-atom resolution and simulated for 600 ns, to compare the dynamics of Ptase$_{SHIP2}$ alone and in the presence of C2$_{SHIP2}$ (Figure 6). The dynamics was quantified in terms of the RMSD and the root mean square fluctuations (RMSF), averaged over the 600 ns simulation. RMSD was calculated with respect to the initial frame, which corresponds to the final coarse-grained binding conformation, converted into an all-atom resolution. Having had an elastic network applied during the coarse-grained simulations, the overall conformation of this reference structure is close to the initial crystal structure (PDB: 5OKM). Previous MD simulations showed that C2$_{SHIP2}$ affects the conformation of loop L4 (residues 674-684) and helices α5-7 (residues 615-643) of Ptase$_{SHIP2}$ [10]. These simulations were done without a lipid membrane, so we tested whether the results could be reproduced in the presence of a lipid membrane. Our simulations confirm this conformational change with SHIP2 bound to a membrane, as the RMSD of those regions vary in the presence or absence of C2$_{SHIP2}$ (Figure 6A). We also confirm that loop L3 of Ptase$_{SHIP2}$ (residues 587-594), which is in the interface between the domains, is less flexible in the presence of C2$_{SHIP2}$, as shown from a decrease in RMSF (Figure 6B). However, C2$_{SHIP2}$ does not change fluctuations of loop L4 and helices α5-7 significantly (Figure 6B), although this was

 doi:10.20944/preprints202302.0282.v1

reported in the simulations without a membrane [10]. Moreover, loop L2 of Ptase$_{SHIP2}$ (residues 531-539) showed a strong reduction in fluctuations in the presence of C2$_{SHIP2}$ (Figure 6B) in our simulations, as opposed to the simulations without a membrane, where the dynamics of L2 increased in the presence of C2 [10]. This is likely due to the fact that L2 is facing the membrane.

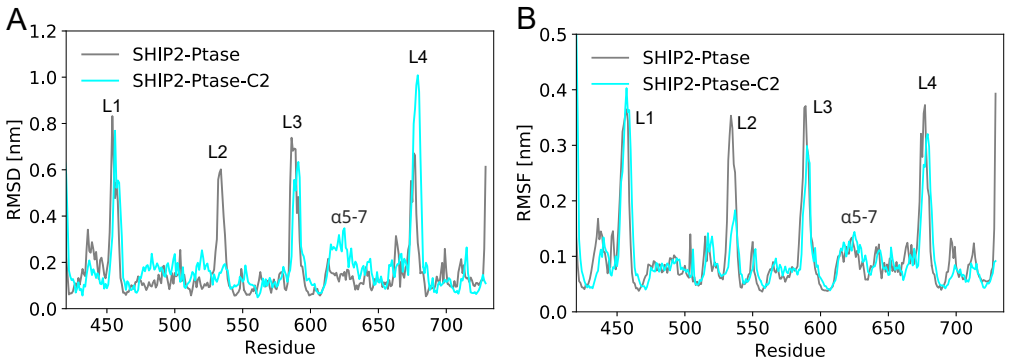

Figure 6. RMSD and RMSF of all-atom simulations of full-length SHIP2 and Ptase$_{SHIP2}$. (A) RMSDs of the Ptase section are calculated per residue as time average over the 600 ns simulations, with respect to the binding poses at 0 ns for Ptase$_{SHIP2}$ (grey) and full-length SHIP2 (Ptase-C2, cyan). Loop L4 (residues 674-684) and helices α5-7 (residues 615-643) are highlighted in orange. (B) Corresponding RMSF.

4. Discussion

In order to probe the different roles of C2 in the phosphatases PTEN and SHIP2, we measured their contributions to the free energy of lipid binding (Figure 4). In PTEN, the C2 and Ptase domains contribute equally to the lipid binding energy, whereas in SHIP2, the binding energy is dominated by the Ptase domain. Moreover, PTEN exhibits a substantially stronger overall membrane binding than SHIP2.

4.1. Negative net charge of the membrane is critical for C2 domain binding

We have previously simulated membrane binding of C2$_{PTEN}$ and C2$_{SHIP2}$ under the same conditions as in the present study, but with a smaller membrane (7 nm x 7 nm versus 12 nm x 12 nm) [6]. With the smaller membrane, the binding energy of C2$_{PTEN}$ was estimated to 78 ± 4 kJ/mol for (compared to 109 ± 1 kJ/mol with the larger membrane), and the binding energy of C2$_{SHIP2}$ was estimated to 23 ± 1 kJ/mol for (compared to 30 ± 1 kJ/mol with the larger membrane), i.e., the energies were estimated to be 30-40 % larger in the 12 nm x 12 nm membrane compared to the previously used 7 nm x 7 nm membrane. This may be due to the increased number of PIP_2 lipids in the larger membrane (in absolute numbers, as molar concentration was 5% in both cases). There were 11 PIP_2 lipids in each leaflet of the 12 nm x 12 nm membrane in the present study versus 4 in the 7 nm x 7 nm membrane [6]. This supports the known biological importance of polyphosphoinositides [28]. When PIP_2 was not present (i.e., PC/PS in anionic membrane), the binding energies were estimated to be 2-3-fold smaller [6]. Negative net charge of the membrane is pivotal, as C2 domains generally do not bind to pure PC membrane, according to all-atom simulations of various C2 domains [6] and experimental binding studies of C2$_{PTEN}$ [29].

4.2. Comparison of experimentally and computationally estimated binding energies

The free energy values we calculated are somewhat overestimated when compared to experimental estimates [29–33]. E.g., wild-type PTEN binding to a PC/PS/PIP_2 (70:29:1) plasma membrane mimic was estimated to have a K_d-value of 0.04 ± 0.01 μM, corresponding to a free energy of -42 ± 1 kJ/mol at 293 K [32]. By contrast, our calculations estimated a free energy value of -163 ± 1 kJ/mol for PTEN binding to a PC/PS/PIP_2 (80:15:5) membrane. Part of this discrepancy may be

 doi:10.20944/preprints202302.0282.v1

ascribed to the higher content of PIP_2 in the simulations compared to the experiment (5 mol% compared to 1 mol%), albeit PS content is lower in the simulations (15 mol% compared to 29 mol%). Moreover, it has recently been shown that the Martini 2 force field is prone to overestimate protein-lipid affinity for amphipathic helices [34], which may be the case for peripheral membrane proteins as well. When converting from coarse-grained to all-atomistic resolution, we saw an increase of the protein-membrane distance for both PTEN and SHIP2 (Figure 5B). Such loosening of the binding pose is in line with an overestimation of the binding energy in the coarse-grained MD simulations, albeit we note that both proteins stayed bound at the membrane in the atomistic simulations.

Thus, while comparison of the absolute free energy values between our calculations and experiments is difficult, we are able to compare trends between them.

4.3. C2 facilitates membrane binding in PTEN

It has been shown experimentally that the C2 domain of PTEN contributes to membrane binding on a PC/PS membrane, with a K_d of 84 ± 9 μM (ΔG = -23 ± 1 kJ/mol) for $C2_{PTEN}$ compared to a K_d 2.9 ± 0.3 μM (ΔG = -31 ± 1 kJ/mol) for full-length PTEN [29]. In contrast, the addition of the C2 domain to a Ptase construct of SHIP2 showed experimentally no increase in binding affinity to PIP_3, but rather a decrease (K_d 30 ± 3 μM for $Ptase_{SHIP2}$ *vs.* K_d 52 ± 4 μM for full-length SHIP2) [30]. This agrees qualitatively with our results, which show that $C2_{SHIP2}$ binds significantly weaker to an anionic phospholipid membrane than $C2_{PTEN}$ (-30 ± 1 kJ/mol for $C2_{SHIP2}$ *vs.* -109 ± 1 kJ/mol for $C2_{PTEN}$). Additionally, our simulations show that the Ptase domain of SHIP2 can bind in its productive conformation without the C2 domain. In contrast, $Ptase_{PTEN}$ must have the C2 domain present to achieve its productive binding conformation.

Interestingly, phosphorylation of the C-terminus of PTEN (i.e. the "C2-end") have previously been shown to allosterically affect PTEN phenotypes [35], suggesting that C2 also acts as an allosteric regulator in PTEN, so C2 play several roles in PTEN.

Our results confirm that for PTEN, the C2 domain facilitates membrane binding and positioning the active site towards its substrate [8,29,36]. However, the results also raise the question: what is the role of the C2 domain in SHIP2?

4.4. C2 allosterically affects catalytic activity in SHIP2

It has been shown by Le Coq et al. that $C2_{SHIP2}$ is essential for cellular function [10], and the authors suggested that $C2_{SHIP2}$ provides allosteric interdomain effects which lead to an increase in the catalytic activity of the Ptase domain. With MD simulations, the authors demonstrated that an interaction between the C2 domain and R649 in the Ptase domain alter the dynamics of helices α5-7 (residues 615-643), and of loop L4 (residues 674-684). The authors proposed that the change in dynamics of L4 by $C2_{SHIP2}$ is essential for catalytic activity by enabling L4 to alter between an open and closed conformation [10]. Here, we did similar analysis, but with SHIP2 bound to a lipid membrane. Our simulations support that the presence of C2 in SHIP2 leads to conformational changes in the L4 loop and the α5-7 helices (Figure 6). However, we did not observe any change of flexibility in these regions. The presence of a lipid membrane quenched the change in dynamics of these regions, and changed dynamics of the L2 loop. However, we confirm the putative role of C2 in SHIP2 as an allosteric regulator of the Ptase domain.

5. Conclusion

Although SHIP2 and PTEN are both phosphatases and contain a catalytic Ptase domain and an adjacent C2 domain, the role of their C2 domains appear to be different. The C2 domain of PTEN participates significantly in membrane binding, and is important for positioning of the active site in the Ptase domain towards the lipid substrate; a role also observed for other C2 domains [37]. In contrast, the C2 domain in SHIP2 bound relatively weakly to anionic phospholipid membranes and the Ptase domain was able to gain the active conformation in the absence of the C2 domain. Therefore, the role of C2 in SHIP2 must be different from the membrane-anchoring role it undertakes in PTEN.

Our simulations suggest that the C2 domain is responsible for allosteric interdomain changes in the L4 loop and in the α5-7 helices, as proposed previously [10]. This allosteric effect is likely to be essential for catalytic activity and can explain why the C2 domain is still essential for protein function in SHIP2.

Author Contributions: AHL, LJ, FN and MS conceived the idea for the project. AHL did the simulations. AHL and LJ did the analysis. AHL and LJ wrote the manuscript with input from all authors.

Acknowledgements: AHL thanks the Carlsberg Foundation (grant CF19-0288) and the Lundbeck Foundation (grant R347-2020-2339) for funding. LHJ thanks UKRI-BBSRC Interdisciplinary Bioscience Doctoral Training Partnership (BB/M011224/1) and the ISIS facility development studentship programme, as well as the Erasmus+ Programme.

References

1. Corbalan-Garcia, S.; Gómez-Fernández, J.C. Signaling through C2 Domains: More than One Lipid Target. *Biochim. Biophys. Acta - Biomembr.* **2014**, *1838*, 1536–1547, doi:10.1016/j.bbamem.2014.01.008.
2. Edimo, E.; Schurmans, S.; Roger, P.P.; Erneux, C. Advances in Biological Regulation SHIP2 Signaling in Normal and Pathological Situations: Its Impact on Cell Proliferation. *Adv. Biol. Regul.* **2014**, *54*, 142–151, doi:10.1016/j.jbior.2013.09.002.
3. Clément, S.; Krause, U.; Desmedt, F.; Tanti, J.F.; Behrends, J.; Pesesse, X.; Sasaki, T.; Penninger, J.; Doherty, M.; Malaisse, W.; et al. The Lipid Phosphatase SHIP2 Controls Insulin Sensitivity. *Nature* **2001**, *409*, 92–97, doi:10.1038/35051094.
4. Li, L.; Ross, A.H. Why Is PTEN an Important Tumor Suppressor? *J. Cell. Biochem.* **2007**, *102*, 1368–1374, doi:10.1002/jcb.21593.
5. Zhang, D.; Aravind, L. Identification of Novel Families and Classification of the C2 Domain Superfamily Elucidate the Origin and Evolution of Membrane Targeting Activities in Eukaryotes. *Gene* **2010**, *469*, 18–30, doi:10.1016/j.gene.2010.08.006.
6. Larsen, A.H.; Sansom, M.S.P. Binding of Ca2+-Independent C2 Domains to Lipid Membranes: A Multi-Scale Molecular Dynamics Study. *Structure* **2021**, *29*, 1200–1213, doi:10.1016/j.str.2021.05.011.
7. Larsen, A.H.; John, L.H.; Sansom, M.S.P.; Corey, R.A. Specific Interactions of Peripheral Membrane Proteins with Lipids: What Can Molecular Simulations Show Us? *Biosci. Rep.* **2022**, *42*, BSR20211406, doi:10.1042/BSR20211406.
8. Lee, J.O.; Yang, H.; Georgescu, M.M.; Cristofano, A. Di; Maehama, T.; Shi, Y.; Dixon, J.E.; Pandolfi, P.; Pavletich, N.P. Crystal Structure of the PTEN Tumor Suppressor: Implications for Its Phosphoinositide Phosphatase Activity and Membrane Association. *Cell* **1999**, *99*, 323–334, doi:10.1016/S0092-8674(00)81663-3.
9. Fiser, A.; Do, R.K.; Sali, A.; Fiser, A.; Kinh, R.; Do, G.; Andrej, S. Modeling of Loops in Protein Structures. *Protein Sci.* **2000**, *9*, 1753–1773, doi:10.1110/ps.9.9.1753.
10. Le Coq, J.; Camacho-Artacho, M.; Velázquez, J.; Santiveri, C.M.; Gallego, L.H.; Campos-Olivas, R.; Dölker, N.; Lietha, D. Structural Basis for Interdomain Communication in SHIP2 Providing High Phosphatase Activity. *Elife* **2017**, *6*, 1–25, doi:10.7554/eLife.26640.
11. Marrink, S.J.; Risselada, H.J.; Yefimov, S.; Tieleman, D.P.; de Vries, A.H. The MARTINI Force Field: Coarse Grained Model for Biomolecular Simulations. *J. Phys. Chem. B* **2007**, *111*, 7812–7824.
12. De Jong, D.H.; Singh, G.; Bennett, W.F.D.; Arnarez, C.; Wassenaar, T.A.; Schäfer, L. V.; Periole, X.; Tieleman, D.P.; Marrink, S.J. Improved Parameters for the Martini Coarse-Grained Protein Force Field. *J. Chem. Theory Comput.* **2013**, *9*, 687–697, doi:10.1021/ct300646g.
13. Kabsch, W.; Sander, C. Dictionary of Protein Secondary Structure: Pattern Recognition of Hydrogen-bonded and Geometrical Features. *Biopolymers* **1983**, *22*, 2577–2637, doi:10.1002/bip.360221211.
14. Wassenaar, T.A.; Ingólfsson, H.I.; Böckmann, R.A.; Tieleman, D.P.; Marrink, S.J. Computational Lipidomics with Insane: A Versatile Tool for Generating Custom Membranes for Molecular Simulations. *J. Chem. Theory Comput.* **2015**, *11*, 2144–2155, doi:10.1021/acs.jctc.5b00209.
15. López, C.A.; Sovova, Z.; Van Eerden, F.J.; De Vries, A.H.; Marrink, S.J. Martini Force Field Parameters for Glycolipids. *J. Chem. Theory Comput.* **2013**, *9*, 1694–1708, doi:10.1021/ct3009655.
16. Berendsen, H.J.C.; Postma, J.P.M.; Van Gunsteren, W.F.; Dinola, A.; Haak, J.R. Molecular Dynamics with Coupling to an External Bath. *J. Chem. Phys.* **1984**, *81*, 3684–3690, doi:10.1063/1.448118.
17. Bussi, G.; Donadio, D.; Parrinello, M. Canonical Sampling through Velocity Rescaling. *J. Chem. Phys.* **2007**, *126*, doi:10.1063/1.2408420.
18. Hess, B.; Bekker, H.; Berendsen, H.J.C.; Fraaije, J.G.E.M. LINCS: A Linear Constraint Solver for Molecular Simulations. *J. Comput. Chem.* **1997**, *18*, 1463–1472, doi:10.1002/(SICI)1096-987X(199709)18:12<1463::AID-JCC4>3.0.CO;2-H.

19. Vickery, O.N.; Stansfeld, P.J. CG2AT2: An Enhanced Fragment-Based Approach for Serial Multi-Scale Molecular Dynamics Simulations. *J. Chem. Theory Comput.* **2021**, *17*, 6472–6482, doi:10.1021/acs.jctc.1c00295.
20. Huang, J.; Rauscher, S.; Nawrocki, G.; Ran, T.; Feig, M.; de Groot, B.L.; Grubmüller, H.; MacKerell, A.D. CHARMM36m: An Improved Force Field for Folded and Intrinsically Disordered Proteins. *Nat. Methods* **2017**, *14*, 71–73, doi:10.1038/nmeth.4067.
21. Darden, T.; York, D.; Pedersen, L. Particle Mesh Ewald: An N·log(N) Method for Ewald Sums in Large Systems. *J. Chem. Phys.* **1993**, *98*, 10089–10092, doi:10.1063/1.464397.
22. Parrinello, M.; Rahman, A. Polymorphic Transitions in Single Crystals: A New Molecular Dynamics Method. *J. Appl. Phys.* **1981**, *52*, 7182–7190, doi:10.1063/1.328693.
23. Kumar, S.; Bouzida, D.; Swendsen, R.H.; Kollman, P.A.; Rosenberg, J.M. The Weighted Histogram Analysis Method for Free-Energy Calculations on Biomolecules. *J. Comput. Chem.* **1992**, *13*, 1011–1021.
24. Hub, J.S.; De Groot, B.L.; Van Der Spoel, D. G_wham - A Free Weighted Histogram Analysis Implementation Including Robust Error and Autocorrelation Estimates. *J. Chem. Theory Comput.* **2010**, *6*, 3713–3720, doi:10.1021/ct100494z.
25. Harris, C.R.; Millman, K.J.; van der Walt, S.J.; Gommers, R.; Virtanen, P.; Cournapeau, D.; Wieser, E.; Taylor, J.; Berg, S.; Smith, N.J.; et al. Array Programming with NumPy. *Nature* **2020**, *585*, 357–362, doi:10.1038/s41586-020-2649-2.
26. Hunter, J.D. Matplotlib: A 2D Graphics Environment. *Comput. Sci. Eng.* **2007**, *9*, 90–95.
27. Song, W.; Corey, R.A.; Ansell, T.B.; Cassidy, C.K.; Horrell, M.R.; Duncan, A.L.; Stansfeld, P.J.; Sansom, M.S.P. PyLipID: A Python Package for Analysis of Protein-Lipid Interactions from Molecular Dynamics Simulations. *J. Chem. Theory Comput.* **2022**, *18*, 1188–1201, doi:10.1021/acs.jctc.1c00708.
28. Hammond, G.R. V.; Balla, T. Polyphosphoinositide Binding Domains: Key to Inositol Lipid Biology. *Biochim Biophys Acta* **2015**, *1851*, 746–758, doi:10.1016/j.bbalip.2015.02.013.Polyphosphoinositide.
29. Das, S.; Dixon, J.E.; Cho, W. Membrane-Binding and Activation Mechanism of PTEN. *Proc. Natl. Acad. Sci. U. S. A.* **2003**, *100*, 7491–7496, doi:10.1073/pnas.0932835100.
30. Le Coq, J.; López Navajas, P.; Rodrigo Martin, B.; Alfonso, C.; Lietha, D. A New Layer of Phosphoinositide-Mediated Allosteric Regulation Uncovered for SHIP2. *FASEB J.* **2021**, *35*, 1–12, doi:10.1096/fj.202100561R.
31. Shenoy, S.S.; Nanda, H.; Lösche, M. Membrane Association of the PTEN Tumor Suppressor: Electrostatic Interaction with Phosphatidylserine-Containing Bilayers and Regulatory Role of the C-Terminal Tail. *J. Struct. Biol.* **2012**, *180*, 394–408, doi:10.1016/j.jsb.2012.10.003.
32. Shenoy, S.; Shekhar, P.; Heinrich, F.; Daou, M.C.; Gericke, A.; Ross, A.H.; Lösche, M. Membrane Association of the PTEN Tumor Suppressor: Molecular Details of the Protein-Membrane Complex from SPR Binding Studies and Neutron Reflection. *PLoS One* **2012**, *7*, doi:10.1371/journal.pone.0032591.
33. Harishchandra, R.K.; Neumann, B.M.; Gericke, A.; Ross, A.H. Biophysical Methods for the Characterization of PTEN/Lipid Bilayer Interactions. *Methods* **2015**, *77*, 125–135, doi:10.1016/j.ymeth.2015.02.004.
34. Van Hilten, N.; Stroh, K.S.; Risselada, H.J. Efficient Quantification of Lipid Packing Defect Sensing by Amphipathic Peptides: Comparing Martini 2 and 3 with CHARMM36. *J. Chem. Theory Comput.* **2022**, *18*, 4503–4514, doi:10.1021/acs.jctc.2c00222.
35. Smith, I.N.; Dawson, J.E.; Eng, C. Comparative Protein Structural Network Analysis Reveals C-Terminal Tail Phosphorylation Structural Communication Fingerprint in PTEN-Associated Mutations in Autism and Cancer. *J. Phys. Chem. B* **2022**, 1DYMMY, doi:10.1021/acs.jpcb.2c06776.
36. Georgescu, M.M.; Kirsch, K.H.; Kaloudis, P.; Yang, H.; Pavletich, N.P.; Hanafusa, H. Stabilization and Productive Positioning Roles of the C2 Domain of PTEN Tumor Suppressor. *Cancer Res.* **2000**, *60*, 7033–7038.
37. Meng, Y.; Sanlidag, S.; Jensen, S.A.; Burnap, S.A.; Struwe, W.B.; Larsen, A.H.; Feng, X.; Mittal, S.; Sansom, M.S.P.; Sahlgren, C.; et al. An N-Glycan on the C2 Domain of JAGGED1 Is Important for Notch Activation. *Sci. Signal.* **2022**, *15*, eabo3507, doi:10.1126/scisignal.abo3507.